Appl. Phys. B 89, 439–445 (2007)
DOI: 10.1007/s00340-007-2865-6

**Applied Physics B**
**Lasers and Optics**

A. JACOB[1,✉]
P. ÖHBERG[2]
G. JUZELIŪNAS[3]
L. SANTOS[1]

# Cold atom dynamics in non-Abelian gauge fields

[1] Institut für Theoretische Physik, Leibniz Universität Hannover, Appelstr. 2, 30167 Hannover, Germany
[2] SUPA, Department of Physics, Heriot-Watt University, Edinburgh, UK
[3] Institute of Theoretical Physics and Astronomy of Vilnius University, A. Goštauto 12, 01108 Vilnius, Lithuania

**Received: 3 July 2007/Revised version: 12 October 2007**
**Published online: 28 November 2007 •** 

**ABSTRACT** The dynamics of ultracold neutral atoms subject to a non-Abelian gauge field is investigated. In particular we analyze in detail a simple experimental scheme to achieve a constant, but non-Abelian gauge field, and discuss in the frame of this gauge field the non-Abelian Aharanov–Bohm effect. In the last part of this paper, we discuss intrinsic non-Abelian effects in the dynamics of cold atomic wavepackets.

**PACS** 03.75.Hh

## 1 Introduction

Gauge potentials, and gauge theories in general, are crucial for the understanding of the fundamental forces between subatomic particles. The simplest example of gauge potentials is the vector potential in the theory of electromagnetism [1], which is an example of an Abelian gauge field. Non-Abelian situations, where the gauge potential is a matrix whose vector components do not commute, are surprisingly scarce in nature. Candidates so far have mainly been restricted to molecular systems [2], which are largely approachable only through spectroscopic means. Other systems are liquid crystals, which show the required non-Abelian symmetries [3, 4].

An elegant derivation and description of the emergence of non-Abelian gauge potentials has been presented by Wilczek and Zee [5], who showed that in the presence of a general adiabatic motion of a quantum system with degenerate states, gauge potentials will appear that are traditionally only encountered in high-energy physics to describe the interactions between elementary particles. Ultracold atomic clouds are particularly promising candidates for realizing such scenarios, since the access to physical parameters is, from an experimental point of view, unprecedented. Extending the ideas of Wilczek and Zee, it was recently proposed that properly tailored laser beams coupled to degenerated internal electronic states can be employed to induce non-Abelian gauge fields in cold-atom experiments [6]. Alternatively, a non-Abelian gauge potential can be constructed in an optical lattice using laser-assisted state sensitive tunnelling [7]. With the implementation of these proposals, ultracold atoms would offer a unique testbed for the analysis of non-trivial non-Abelian effects on the quantum dynamics of multicomponent wavepackets.

In this paper, we investigate the wave packet dynamics of a cloud of ultracold atoms in the presence of a non-Abelian gauge potential. In Sect. 2 we discuss how this undoubtedly rather exotic scenario can be envisaged in a sample of cold atoms where the internal electronic energy levels are addressed by laser fields with a nontrivial spatial phase and intensity distribution. This setup opens up a number of new scenarios for ultracold gases, allowing for the study of non-Abelian atom optics, which naturally ties together optical and magnetic effects. Remarkably, as shown in Sect. 2, even very simple laser arrangements may induce non-trivial cold-atom dynamics. As a first example of this non-trivial dynamics, we discuss in Sect. 3 a possible optical tweezer experiment including a non-Abelian flux, for which the population transfer between internal states crucially depends on the path taken (non-Abelian Aharonov–Bohm effect). This effect resembles indeed what one would expect from scattering protons onto a non-Abelian flux line where the proton can be transferred into a neutron [8]. The tweezer experiment discussed in Sect. 3 just involves the internal-state dynamics, without exploring the rich dynamics resulting from the interplay between external and internal degrees of freedom in non-Abelian gauge fields. Section 4 is devoted to the analysis of this interplay. In particular, we show that the dynamics of cold-atom wavepackets can be significantly affected by intrinsically non-Abelian effects, which are crucially dependent on the initial momentum distribution of the wavepacket. We consider in particular the relevant examples of wavepacket propagation and wavepacket reflection at an atomic mirror. Finally, we conclude in Sect. 5.

## 2 Laser-induced non-Abelian gauge fields

In a recent paper [6] it was shown that a non-Abelian gauge potential can be constructed in the presence of nontrivial light fields coupled to degenerate electronic states of cold atoms. For this we consider atoms with multiple internal states, see Fig. 1. For a fixed position $\boldsymbol{r}$ the internal Hamiltonian $\hat{H}_0(\boldsymbol{r})$ including the laser interaction can be diagonalized to give a set of 4 dressed states $|\chi_n(\boldsymbol{r})\rangle$ with eigen-

✉ Fax: +49-511-762-3023, E-mail: andreas@itp.uni-hannover.de

values $\varepsilon_n(\boldsymbol{r})$, where $n = 1, 2, 3, 4$. The full quantum state of the atom describing both internal and motional degrees of freedom can then be expanded in terms of the dressed states according to $|\Phi\rangle = \sum_{n=1}^{4} \Psi_n(\boldsymbol{r})\,|\chi_n(\boldsymbol{r})\rangle$. If there are two degenerate dressed states and we can neglect the transitions to the other states we obtain a coupled two level system of the form

$$\mathrm{i}\hbar\frac{\partial}{\partial t}\tilde{\Psi} = \left[\frac{1}{2m}(-\mathrm{i}\hbar\nabla - \boldsymbol{A})^2 + V + \Phi\right]\tilde{\Psi}\,, \tag{1}$$

where the $2\times 2$ potentials are given by

$$V_{n,m} = \varepsilon_n(\boldsymbol{r})\,\delta_{n,m} + \langle\chi_n(\boldsymbol{r})|V(\boldsymbol{r})|\chi_m(\boldsymbol{r})\rangle\,, \tag{2}$$

$$\boldsymbol{A}_{n,m} = \mathrm{i}\hbar\langle\chi_n(\boldsymbol{r})\,|\nabla\chi_m(\boldsymbol{r})\rangle\,. \tag{3}$$

$$\Phi_{n,m} = \frac{\hbar^2}{2m}\left(\langle\nabla\chi_n\,|\nabla\chi_m\rangle + \sum_{k=1}^{2}\langle\chi_n\,|\nabla\chi_k\rangle\langle\chi_k|\nabla\chi_m\rangle\right)\,. \tag{4}$$

The reduced $2\times 2$ matrix $\boldsymbol{A}$ is sometimes referred to as the Berry connection and is related to a curvature (an effective "magnetic" field) $\boldsymbol{B}$ as

$$B_i = \frac{1}{2}\varepsilon_{ikl}F_{kl}, \quad F_{kl} = \partial_k A_l - \partial_l A_k - \frac{\mathrm{i}}{\hbar}\left[A_k, A_l\right]\,. \tag{5}$$

Note that the term $\frac{1}{2}\varepsilon_{ikl}\left[A_k, A_l\right] = (\boldsymbol{A}\times\boldsymbol{A})_i$ does not vanish in general, since the vector components of $\boldsymbol{A}$ do not necessarily commute. In fact, this term reflects the non-Abelian character of the gauge potentials.

To construct a scheme of laser–atom interactions that leads to a $U(2)$ gauge potential we need degenerate (or nearly degenerate) dressed states. Such a condition is fulfilled e.g., for the tripod system shown in Fig. 1. A truly non-Abelian situation emerges if the matrices $\{A_x, A_y, A_z, \Phi\}$ do not commute. For this it is necessary that the off-diagonal element $\mathrm{i}\hbar\langle\chi_1(\boldsymbol{r})\,|\nabla\chi_2(\boldsymbol{r})\rangle$ is non-zero. The Hamiltonian of the tripod system reads in interaction representation as [6, 9, 10]

$$\hat{H}_0 = -\hbar\left(\Omega_1\,|0\rangle\langle 1| + \Omega_2\,|0\rangle\langle 2| + \Omega_3\,|0\rangle\langle 3|\right) + H.c. \tag{6}$$

Parameterizing the Rabi-frequencies $\Omega_\mu$ with angle and phase variables according to $\Omega_1 = \Omega\,\sin\theta\,\cos\varphi\,\mathrm{e}^{\mathrm{i}S_1}$, $\Omega_2 = \Omega\,\sin\theta\,\sin\varphi\,\mathrm{e}^{\mathrm{i}S_2}$, $\Omega_3 = \Omega\,\cos\theta\,\mathrm{e}^{\mathrm{i}S_3}$, where $\Omega = \sqrt{|\Omega_1|^2 + |\Omega_2|^2 + |\Omega_3|^2}$, the adiabatic dark states read

$$|D_1\rangle = \sin\varphi\,\mathrm{e}^{\mathrm{i}S_{31}}|1\rangle - \cos\varphi\,\mathrm{e}^{\mathrm{i}S_{32}}|2\rangle\,, \tag{7}$$

$$|D_2\rangle = \cos\theta\cos\varphi\,\mathrm{e}^{\mathrm{i}S_{31}}|1\rangle + \cos\theta\sin\varphi\,\mathrm{e}^{\mathrm{i}S_{32}}|2\rangle - \sin\theta|3\rangle\,, \tag{8}$$

with $S_{ij} = S_i - S_j$.

The gauge potential depends on the gradient of the dark states:

$$\begin{aligned}
\boldsymbol{A}_{11} &= \hbar\left(\cos^2\varphi\nabla S_{23} + \sin^2\varphi\nabla S_{13}\right)\,,\\
\boldsymbol{A}_{12} &= \hbar\cos\theta\left(\frac{1}{2}\sin(2\varphi)\nabla S_{12} - \mathrm{i}\nabla\varphi\right)\,,\\
\boldsymbol{A}_{22} &= \hbar\cos^2\theta\left(\cos^2\varphi\nabla S_{13} + \sin^2\varphi\nabla S_{23}\right)
\end{aligned} \tag{9}$$

and

$$\begin{aligned}
\Phi_{11} &= \frac{\hbar^2}{2m}\sin^2\theta\left(\frac{1}{4}\sin^2(2\varphi)(\nabla S_{12})^2 + (\nabla\varphi)^2\right)\\
\Phi_{12} &= \frac{\hbar^2}{2\,\mathrm{m}}\sin\theta\left(\frac{1}{2}\sin(2\varphi)\nabla S_{12} - \mathrm{i}\nabla\varphi\right)\\
&\quad\times\left(\frac{1}{2}\sin(2\theta)(\cos^2\varphi\nabla S_{13} + \sin^2\varphi\nabla S_{23}) - \mathrm{i}\nabla\theta\right)\\
\Phi_{22} &= \frac{\hbar^2}{2\,\mathrm{m}}\\
&\quad\times\left(\frac{1}{4}\sin^2(2\theta)\left(\cos^2\varphi\nabla S_{13} + \sin^2\varphi\nabla S_{23}\right)^2 + (\nabla\theta)^2\right)\,.
\end{aligned} \tag{10}$$

This provides a remarkable versatility. Recent advances in shaping both the phase and the intensity of light beams make it possible to choose practically any shape of the gauge potential provided the corresponding light field obeys Maxwell's equations. This is certainly the case in a two-dimensional geometry, but light beams can also be tailored [11, 12] in three dimensions. In the Abelian case, a non-zero effective magnetic field is obtained if there is a relative angular momentum between the two light beams and the intensity ratio is spatially dependent [13–15].

Surprisingly, the generation of a non-Abelian gauge field does not require any elaborate shaping of the three laser beams employed. This is indeed the case if we choose the configuration shown in Fig. 1. Three plane-wave laser beams are used. Two lasers of equal intensity are counter-propagating in the $x$-direction with wave vector $\kappa$ while the third one (of double intensity) propagates in the $y$-direction also with a wave vector $\kappa$. With this arrangement, $\varphi = \pi/4$, and $\theta = \pi/4$ in the expressions above. The resulting vector potential is of the form:

$$\boldsymbol{A} = \hbar\kappa\begin{pmatrix} -\boldsymbol{e}_y & \boldsymbol{e}_x/\sqrt{2} \\ \boldsymbol{e}_x/\sqrt{2} & -\boldsymbol{e}_y/2 \end{pmatrix}\,, \tag{11}$$

whereas

$$V + \Phi = \begin{pmatrix} V_1 + \frac{\hbar^2\kappa^2}{4m} & 0 \\ 0 & (V_1+V_3)/2 + \frac{\hbar^2\kappa^2}{8m} \end{pmatrix}\,. \tag{12}$$

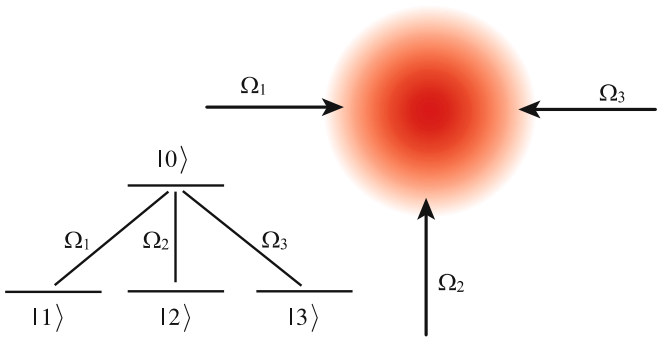


**FIGURE 1** The tripod coupling scheme forms two degenerate dark states with a non-adiabatic coupling. The three laser beams $\Omega_i$ $i = 1, 2, 3$ are arranged as two counter propagating *beams* ($\Omega_1$ and $\Omega_2$) and one *beam* ($\Omega_3$) (of double intensity) in the perpendicular direction

By choosing the laser detuning such that $V_3 - V_1 = \hbar^2\kappa^2/4m$ we obtain a scalar potential proportional to the unit matrix, $V + \Phi = V_1 \mathrm{I}$. Therefore the scalar potential can be safely neglected as far as the wavepacket dynamics is concerned.

## 3 Non-Abelian Aharonov–Bohm effect

In [7], it was proposed that non-Abelian gauge fields created in lattices can be employed to construct non-Abelian atom interferometers. However, the read-out of any non-Abelian atom interferometer may be crucially handicapped by the non-trivial interplay between external and internal degrees of freedom in the wavepacket dynamics of atoms in non-Abelian gauge fields (see Sect. 4). However, this coupling between external and internal dynamics may be prevented by considering atoms trapped in mobile optical tweezers. If the tweezer potential is strong enough, the system may be investigated in the so-called single-mode approximation, in which both components share exactly the same center-of-mass wavepacket. As a consequence, the non-Abelian gauge field will just affect the internal dynamics of the atoms. In the following we envisage an experiment in which a cloud of ultracold atoms is trapped by an optical tweezer under the conditions discussed above. When moving in the $xy$ plane, the atoms experience the gauge potential given by (11). We consider the case where the atoms are moved in the $x$ and $y$ direction (Fig. 2) along two different paths: (clock-wise, $L$) from $(0, 0)$ to $(0, s)$ and then from $(0, s)$ to $(s, s)$; (anti clockwise, $R$) from $(0, 0)$ to $(s, 0)$ and then from $(s, 0)$ to $(s, s)$. The initial state of the atom is assumed to be a linear superposition of both dark states:

$$|\Psi(0)\rangle = \cos(\eta)\,|D_1\rangle + \mathrm{e}^{\mathrm{i}\varphi}\sin(\eta)\,|D_2\rangle \tag{13}$$

where $\eta$ is the mixing angle, and $\varphi$ is a relative phase. The dynamics of the two level system obviously depends on the initial state, but more importantly, the final populations of the two dark states depend on which path is taken. After performing the clockwise path the atoms are in the state

$$|\Psi_{\mathrm{L}}\rangle = \mathrm{e}^{\mathrm{i}\hat{A}_x s/\hbar}\,\mathrm{e}^{\mathrm{i}\hat{A}_y s/\hbar}\,|\Psi(0)\rangle = c_1^L\,|D_1\rangle + c_2^L\,|D_2\rangle \tag{14}$$

whereas after performing the anti clockwise path we have:

$$|\Psi_R\rangle = \mathrm{e}^{\mathrm{i}\hat{A}_y s/\hbar}\,\mathrm{e}^{\mathrm{i}\hat{A}_x s/\hbar}\,|\Psi(0)\rangle = c_1^R\,|D_1\rangle + c_2^R\,|D_2\rangle\,. \tag{15}$$

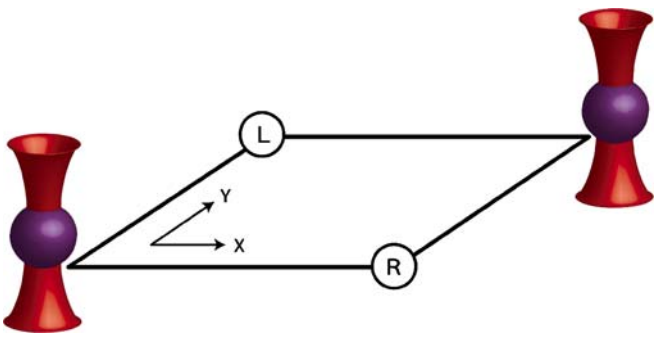


**FIGURE 2** The envisaged experiment. An optical tweezer moves the cloud of atoms along the left ($L$) path or the right ($R$) path. The final dark state population will depend on which path is taken

Using the vector potential given by (11), a straight forward calculation yields

$$c_1^L = \mathrm{e}^{-\mathrm{i}\kappa s}\cos\left(\frac{\kappa s}{\sqrt{2}}\right)\cos(\eta) + \mathrm{i}\,\mathrm{e}^{\mathrm{i}(\varphi-\kappa s/2)}\sin\left(\frac{\kappa s}{\sqrt{2}}\right)\sin(\eta) \tag{16}$$

$$c_2^L = \mathrm{i}\,\mathrm{e}^{-\mathrm{i}\kappa s}\sin\left(\frac{\kappa s}{\sqrt{2}}\right)\cos(\eta) + \mathrm{e}^{\mathrm{i}(\varphi-\kappa s/2)}\cos\left(\frac{\kappa s}{\sqrt{2}}\right)\sin(\eta) \tag{17}$$

$$c_1^R = \mathrm{e}^{-\mathrm{i}\kappa s}\left(\cos\left(\frac{\kappa s}{\sqrt{2}}\right)\cos(\eta) + \mathrm{i}\,\mathrm{e}^{\mathrm{i}\varphi}\sin\left(\frac{\kappa s}{\sqrt{2}}\right)\sin(\eta)\right) \tag{18}$$

$$c_2^R = \mathrm{e}^{-\mathrm{i}\kappa s/2}\left(\mathrm{i}\sin\left(\frac{\kappa s}{\sqrt{2}}\right)\cos(\eta) + \mathrm{e}^{\mathrm{i}\varphi}\cos(\frac{\kappa s}{\sqrt{2}})\sin(\eta)\right)\,. \tag{19}$$

Figure 3 shows the final population difference between the two dark states for both paths as a function of the path length $\kappa s$. It becomes clear that the outcome of choosing the $L$ or $R$ path can be very different. We stress that this effect is not directly linked to the appearance of off-diagonal terms in the

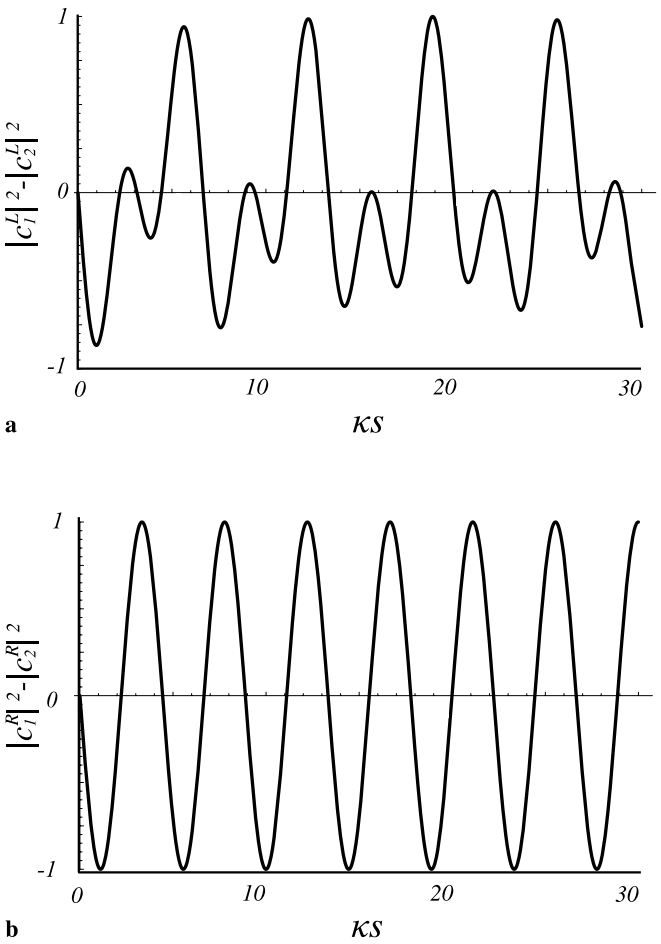


**FIGURE 3** The difference in the populations in the two dark states depends on which path is taken. (**a**) shows the total difference $|c_1^L|^2 - |c_2^L|^2$ as a function of the path length $\kappa\sigma$, whereas in (**b**) we depict $|c_1^R|^2 - |c_2^R|^2$. We assume as initial condition $\eta = \pi/4$, and $\varphi = \pi/2$

corresponding matrices of the vector potential, but rather it is inherently due to the non-Abelian character of the matrices $\hat{A}_x$ and $\hat{A}_y$. This effect is remarkably similar to the scattering of protons onto a non-Abelian flux line, where a conversion of the proton into a neutron is anticipated [8]. A more complete picture is obtained by defining the pseudo spin $\boldsymbol{S}(c_1^{L,R}, c_2^{L,R})$ as

$$S_x = \frac{1}{2\mathrm{i}}\left(c_1 {c_2}^* - {c_1}^* c_2\right) \tag{20}$$

$$S_y = \frac{1}{2}\left(c_1 {c_2}^* + {c_1}^* c_2\right) \tag{21}$$

$$S_z = \frac{1}{2}\left(|c_1|^2 - |c_2|^2\right) . \tag{22}$$

With the pseudo spin representation we can follow the rotation of the spin vector as a function of the position along the different paths. This is shown in Fig. 4 where the spin vector is seen to follow circular paths whose orientation changes when the direction of the atoms in real space changes. The role of the initial state is now immediately clear. Only a superposition between $|D_1\rangle$ and $|D_2\rangle$ will result in a different final state of $\boldsymbol{S}$ as a function of taking either the $L$ or $R$ path. Note in contrast to the previously considered laser-driven population transfer for tripod atoms [9, 10] here the non-Abelian dynamics is due to the time-dependence of the phases of light fields "seen" by moving atoms rather than due to the time-dependence of the intensities of laser pulses.

## 4 Wavepackets in free space

The non-Abelian Aharonov–Bohm effect is a striking example where the internal dynamics of a two-level system is highly nontrivial. A question not often addressed in the context of non-Abelian systems is the dynamics of a wave packet. This situation is clearly more complex compared to the previous non-Abelian Aharonov–Bohm scenario where an adiabatic motion with respect to center-of-mass excitations and shape oscillations was assumed. We now have to fully take into account the coupled internal and external degrees of freedom.

In the following we discuss the evolution of a cold atomic wavepacket in the presence of a non-Abelian gauge field $\hat{A} = \{\hat{A}_x, \hat{A}_y, 0\}$. We consider that the atomic gas is sufficiently dilute, and hence in this paper we neglect the effects of the interatomic interactions. We restrict ourselves to the case in which both matrices $\hat{A}_x$ and $\hat{A}_y$ are space-independent. In order to simplify the discussion below, we consider $\hat{A}_j = \hbar\kappa\hat{M}_j$, with $j = x, y$, where $\kappa$ has units of

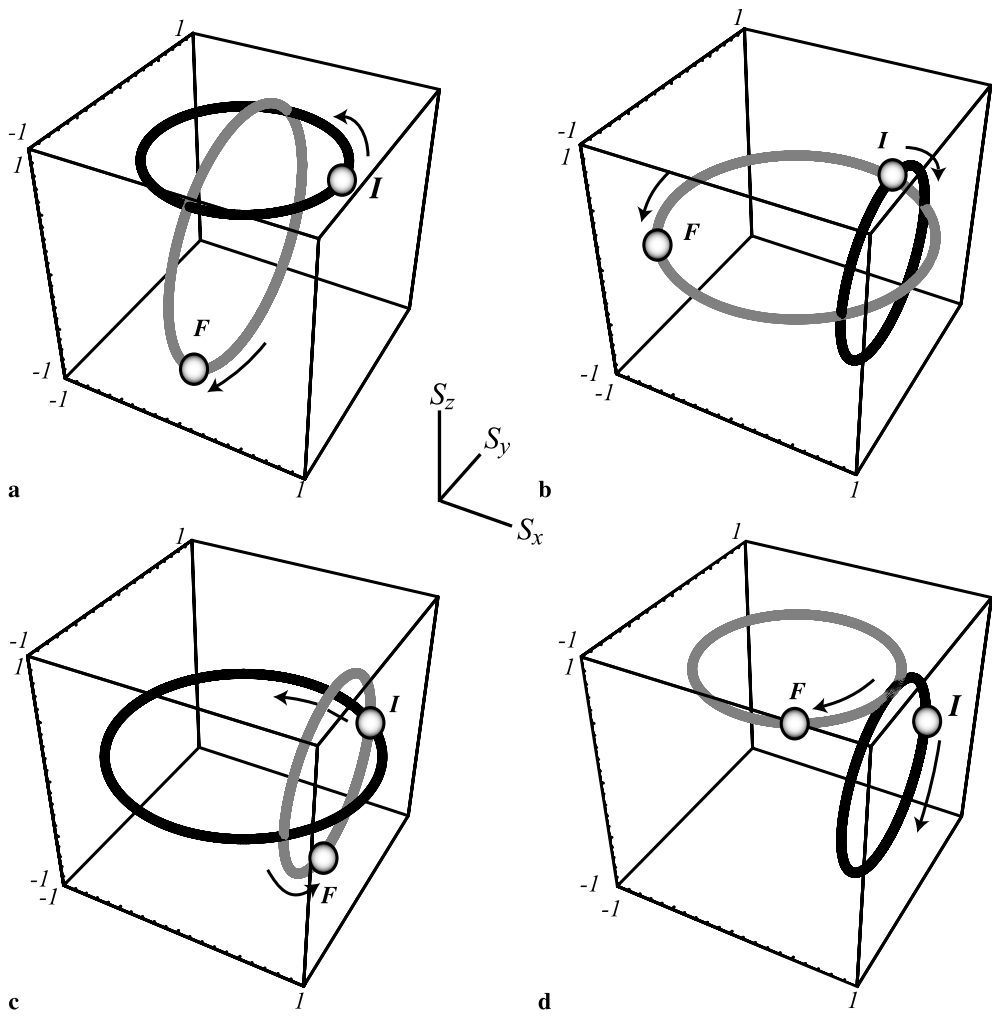


**FIGURE 4** The pseudo spin trajectories depend on the initial state and which path is taken: (**a**) Left path with $\eta = \pi/8, \varphi = 0$, (**b**) Right path with $\eta = \pi/8, \varphi = 0$, (**c**) Left path with $\eta = \pi/4, \varphi = \pi/4$, (**d**) Right path with $\eta = \pi/4, \varphi = \pi/4$. The spheres in each figure indicate the initial state ($I$) and the final state ($F$). The *black circle* is always the path first embarked on. In all cases we have chosen $\kappa s = 34.5$. This will cause the spin vector to traverse the circular paths several times in each plane

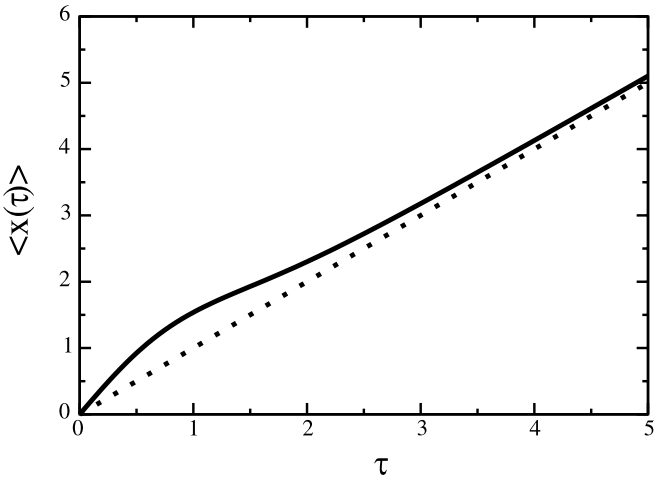


**FIGURE 5** Evolution of the center-of-mass coordinate $\langle x\rangle$ in units of $\sqrt{2}\Delta p/\hbar$, as a function of $\tau = \Delta p\kappa t/\sqrt{2}m$, for $\hat{A}_x = \hbar\kappa\hat{\sigma}_x$, and $\hat{A}_y = \hbar\kappa\hat{\sigma}_z$, $\eta = \pi/4$, $\varphi = 0$. The *dashed line* is the function $f(\tau) = \tau$. For short times, the nonlinear evolution of the center-of-mass becomes clear

wavenumber, and $\hat{M}_j^2 = \hat{1}$. We assume as well that the scalar potential may be considered as a multiple of the identity matrix (as discussed above). Removing unimportant global energy shifts, the Hamiltonian for a free particle becomes

$$\hat{H} = -\frac{\hbar^2}{2m}\nabla^2\hat{1} - \mathrm{i}\frac{\hbar^2\kappa}{m}\left(\hat{M}_x\frac{\partial}{\partial x} + \hat{M}_y\frac{\partial}{\partial y}\right). \tag{23}$$

The atomic wavepacket can be represented by a spinorial wavefunction of the form

$$\boldsymbol{\Psi}(\boldsymbol{r}, t) = \int \mathrm{d}\boldsymbol{p}\, \mathrm{e}^{\mathrm{i}\boldsymbol{p}\cdot\boldsymbol{r}/\hbar}\boldsymbol{\Phi}(\boldsymbol{p}, t)\,. \tag{24}$$

Thus, we have

$$\hat{H}\Psi(\boldsymbol{r}, t) = \int \mathrm{d}\boldsymbol{p}\hat{H}_p(\boldsymbol{p})\boldsymbol{\Phi}(\boldsymbol{p}, t)\,\mathrm{e}^{\mathrm{i}\boldsymbol{p}\cdot\boldsymbol{r}/\hbar}\,, \tag{25}$$

where

$$\hat{H}_p(\boldsymbol{p}) \equiv \frac{p^2}{2m}\hat{1} + \frac{\hbar\kappa}{m}\left(\hat{M}_x p_x + \hat{M}_y p_y\right). \tag{26}$$

Hence, for any given $\boldsymbol{p}$ the equation of motion $\mathrm{i}\hbar\dot{\boldsymbol{\Phi}}(\boldsymbol{p}, t) = \hat{H}_p(\boldsymbol{p})\Phi(\boldsymbol{p}, t)$ yields $\boldsymbol{\Phi}(\boldsymbol{p}, t) = \exp\left[\mathrm{i}\hat{H}_p(\boldsymbol{p})t/\hbar\right]\boldsymbol{\Phi}(\boldsymbol{p}, t = 0)$. This evolution can be analytically obtained after diagonalizing the matrix $\hat{H}_p(\boldsymbol{p})$ for every $\boldsymbol{p}$.

We are interested in comparing the wavepacket evolution in the presence of Abelian and non-Abelian fields. If the fields are Abelian, i.e., $\left[\hat{M}_x, \hat{M}_y\right] = 0$, then we may find a common eigenbasis for both operators, in which $\hat{M}_j = \mathrm{diag}\{\lambda_j^+, \lambda_j^-\}$. As a consequence, the eigenvectors $\boldsymbol{\xi}_\pm$ of $\hat{H}_p(\boldsymbol{p})$ are independent of $\boldsymbol{p}$, and the total wavefunction is at any time a linear combination of the form $\boldsymbol{\Phi}(\boldsymbol{r}, t) = \Phi_+(\boldsymbol{r}, t)\boldsymbol{\xi}_+ + \Phi_-(\boldsymbol{r}, t)\boldsymbol{\xi}_-$, where

$$\Phi_\pm(\boldsymbol{r}, t) = \mathrm{e}^{-\mathrm{i}\varphi_\pm}\int \mathrm{d}\boldsymbol{p}\,\mathrm{e}^{-\mathrm{i}\frac{p^2 t}{2m\hbar}}\,\mathrm{e}^{\mathrm{i}\boldsymbol{p}\cdot\boldsymbol{r}/\hbar}\Psi_\pm\left(\boldsymbol{p} - \boldsymbol{\eta}^\pm, t = 0\right), \tag{27}$$

with $\boldsymbol{\eta}^\pm = \hbar\kappa(\lambda_x^\pm, \lambda_y^\pm)$, and $\varphi_\pm = \frac{(\eta^\pm)^2 t}{2m\hbar} + \boldsymbol{\eta}^\pm\cdot\boldsymbol{r}/\hbar$. Hence, the wavepacket evolution can be considered as an independent scalar evolution for the wavepackets in each component. In particular, it may be easily shown that the center-of-mass position of the wavepacket $\Phi_\pm(\boldsymbol{r}, t)$ grows linearly in time with a velocity $\left(\langle\boldsymbol{p}\rangle + \boldsymbol{\eta}^\pm\right)/m$. Hence, the two wavepackets tend to separate during the time evolution.

The picture changes completely if $\left[\hat{M}_x, \hat{M}_y\right] \neq 0$. In this case the eigenvectors of $\hat{H}_p(\boldsymbol{p})$ do depend on the momentum $\boldsymbol{p}$ considered, and hence the time-evolution of the wavepacket depends in a non-trivial way on the momentum distribution of the original wavepacket. We analyze in particular the center-of-mass (CM) motion of the wavepacket. The $x$-coordinate of the CM after a given time $t$ is better calculated in the momentum representation: $\langle x\rangle_t = \langle\mathrm{i}\hbar\partial/\partial p_x\rangle_t = \langle\mathrm{e}^{\mathrm{i}\hat{H}t/\hbar}\mathrm{i}\hbar\partial/\partial p_x\,\mathrm{e}^{-\mathrm{i}\hat{H}t/\hbar}\rangle_0$, where we have employed the Heisenberg picture. One can then easily obtain that:

$$\langle x\rangle_t = \langle x\rangle_0 + \frac{t}{m}\langle p_x\rangle_0 + \left\langle \mathrm{e}^{\mathrm{i}\hat{O}}\mathrm{i}\hbar\frac{\partial}{\partial p_x}\left[\mathrm{e}^{-\mathrm{i}\hat{O}}\right]\right\rangle_0, \tag{28}$$

where $\hat{O} = (\kappa t/m)(\hat{M}_x p_x + \hat{M}_y p_y)$. The last term in the previous equation leads to non-trivial effects, which are easily illustrated by considering the particular example $\hat{M}_x = \hat{\sigma}_x$, $\hat{M}_y = \hat{\sigma}_z$:

$$\langle x\rangle_t = \langle x\rangle_0 + \frac{t}{m}\langle p_x\rangle_0 + \frac{\hbar\kappa t}{m}\left\{\langle c^2\hat{\sigma}_x + sc\hat{\sigma}_z\rangle_0 + \left\langle\frac{\sin 2q}{2q}s^2\hat{\sigma}_x - \frac{\sin 2q}{2q}sc\hat{\sigma}_z - \frac{\sin^2 q}{q}s\hat{\sigma}_y\right\rangle_0\right\}, \tag{29}$$

where $c = p_x/p, s = p_y/p, q = \kappa t p/m$, and $p^2 = p_x^2 + p_y^2$. Let us consider an initial Gaussian wavepacket

$$\boldsymbol{\Psi}(\boldsymbol{r}) = \Psi(\boldsymbol{r})\begin{pmatrix}\cos\eta\,\mathrm{e}^{\mathrm{i}\varphi/2}\\ \sin\eta\,\mathrm{e}^{-\mathrm{i}\varphi/2}\end{pmatrix},$$

where $\Psi(\boldsymbol{r})$ is a Gaussian centered in $x = y = 0$ and with the Fourier transform $\Phi(\boldsymbol{p}) \sim \exp(-p^2/\Delta p^2)$. Then:

$$\langle x\rangle_\tau = \frac{\hbar}{\sqrt{2}\Delta p}\tau\left[1 + \frac{\sqrt{\pi}}{2}\frac{e^{-\tau^2}}{\tau}\mathrm{erfi}(\tau)\right]\sin 2\eta\cos\varphi\,, \tag{30}$$

where erfi is the imaginary error function, and $\tau = \frac{\Delta p\kappa}{\sqrt{2}m}t$. Note, that contrary to the Abelian case, we have two inherently non-Abelian effects. On one hand, the evolution of the center-of-mass motion is in general a non-trivial nonlinear function of time. However, for $\tau \gg 1$, a linear behavior $\langle x\rangle_\tau \simeq \frac{\hbar}{\sqrt{2}\Delta p}\tau$ is recovered, i.e., there is a characteristical transient stage where an inherently non-Abelian-induced nonlinear CM evolution occurs (see Fig. 5). On the other hand, contrary to the Abelian (or scalar) evolution, the evolution of the CM motion depends on the initial width $\Delta p$ of the momentum distribution. This effect can be traced back to the dependence of the eigenstates $\boldsymbol{\xi}_\pm$ on $\boldsymbol{p}$.

A third effect can be observed if we consider a Gaussian wavepacket with an initial $\langle p_y\rangle_0 \neq 0$. In this case, if $\langle p_x\rangle_0 = 0$,

one obtains:

$$\langle x\rangle_t = \frac{\hbar\kappa}{t}\left[1 - \langle\left(\frac{\sin 2q}{2q} - 1\right)\frac{p_y^2}{p^2}\rangle_0\right]\sin 2\eta\cos\varphi\,. \qquad (31)$$

Hence the $x$-dynamics depends on the momentum distribution in the $y$-direction, contrary to the case of Abelian evolution.

Note that the details of the momentum distribution play a very important role in the wavepacket evolution in non-Abelian gauge fields. Obviously, if $|\langle\boldsymbol{p}\rangle| \gg \kappa$ the non-Abelian effects become negligible. But even if $|\langle\boldsymbol{p}\rangle| \lesssim \kappa$, an Abelian evolution is recovered if $\Delta p \ll \kappa$, i.e., the non-Abelian effects are clearer for wavepackets which at $t = 0$ are localized in space with uncertainties $\lesssim 1/\kappa$. The latter effect may be explained, because if $\Delta p \ll \hbar\kappa$ then $\hat{H}_p$ may be (to a good approximation) simultaneously diagonalized for all relevant values of $\boldsymbol{p}$ in the distribution, and hence again two separated wavepackets as those for the Abelian evolution are recovered. In addition, it is important to realize that the particular evolution also depends on the initial spinor configuration of the wavepacket (although this dependence is not inherently non-Abelian since it also occurs in the Abelian evolution).

Figure 6 shows the results of our numerical simulations of the wavepacket evolution for the gauge field discussed above. Note that (contrary to the usual Abelian (or scalar) evolution), there is a stark difference in the evolution of the shape of the wavepacket for different values of the momentum spreading $\Delta p/\kappa$.

The non-Abelian character of the gauge field also leads to interesting effects in the reflection of atomic wavepackets. Ultracold atomic wavepackets can be reflected at laser or magnetic mirrors [16–18]. For typical situations, the reflection of the center-of-mass of the wavepacket can be considered as specular, i.e., the angle of reflection of the wavepacket with the normal vector of the mirror is exactly minus the angle of incidence of the original wavepacket. Mathematically, the reflection can be considered as the superposition (in absence of mirror) of the original wavepacket and an image wavepacket travelling with opposite momentum and with a dephase $\pi$. For the case of wavepackets in non-Abelian gauge fields, the effect of the mirror cannot be mimicked by this image picture (since contrary to the scalar case, a sinusoidal solution is not an eigenstate of $\hat{H}_p$). As a consequence, the intuitive specular-reflection picture must be revised in the case of wavepackets in non-Abelian gauge fields, even for the cases discussed below in which both internal components experience exactly the same mirror potential.

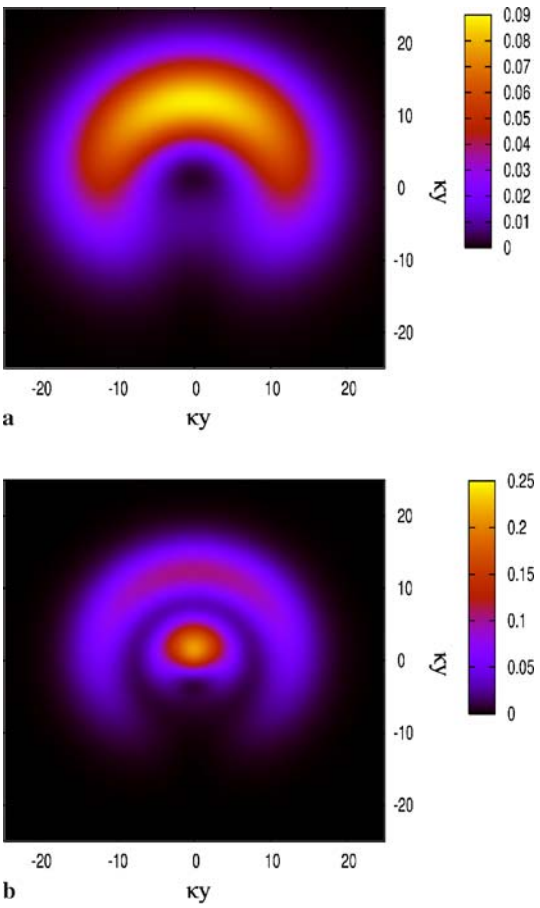


**FIGURE 6** Total density after $t = 10(2m/\hbar\kappa^2)$, for (**a**) $\Delta p = 0.2\hbar\kappa$ and (**b**) $\Delta p = 0.6\hbar\kappa$. At $t = 0$, $\eta = 0$, $\varphi = 0$ and $\langle\boldsymbol{p}\rangle = 0$. In the strong non-Abelian case, the wave packet expands asymmetrically. In an Abelian situation with a radially symmetric effective magnetic field, the expansion would be symmetric

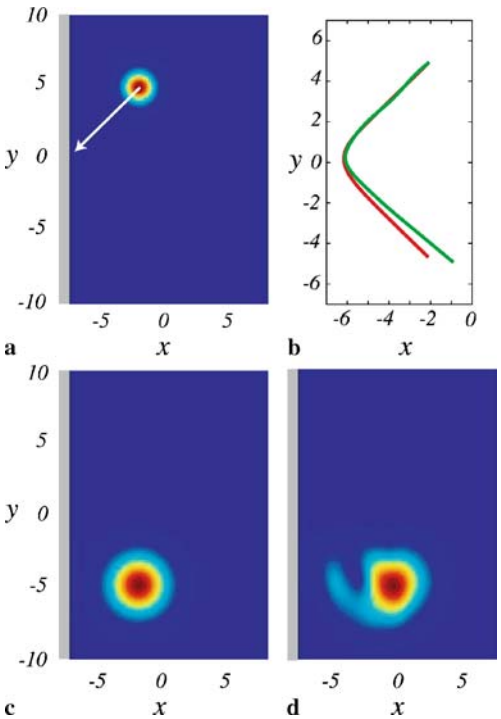


**FIGURE 7** The reflection dynamics of a non-Abelian wave packet compared to a zero gauge field situation. The reflection takes place at $x = -7$ where a steep potential is envisaged (*gray area*). The parameters were chosen to be $\kappa = 1$, $\Delta p = 1$ and initial momentum $\boldsymbol{p}_0 = -\frac{8}{\sqrt{2}}(\hat{\boldsymbol{x}} + \hat{\boldsymbol{y}})$. (**a**) The initial density distribution of the atomic cloud. The initial momentum kick is indicated by the *arrow*. (**b**) The non-Abelian path of the center-of-mass, the inner (*green*) path, for the reflection is clearly different from the standard wave packet reflection with $\kappa = 0$ (*red outer path*). (**c**) A snapshot of the wave packet at the time corresponding to the mirror image with respect to the $x$-axis. For $\kappa = 0$, the reflected angle is the same as the incident angle. (**d**) A snapshot of the wave packet at the same time as in (**c**). For the non-Abelian case, the reflection dynamics is highly non-trivial where the center-of-mass path no longer is described by an incident angle equal to the reflected angle

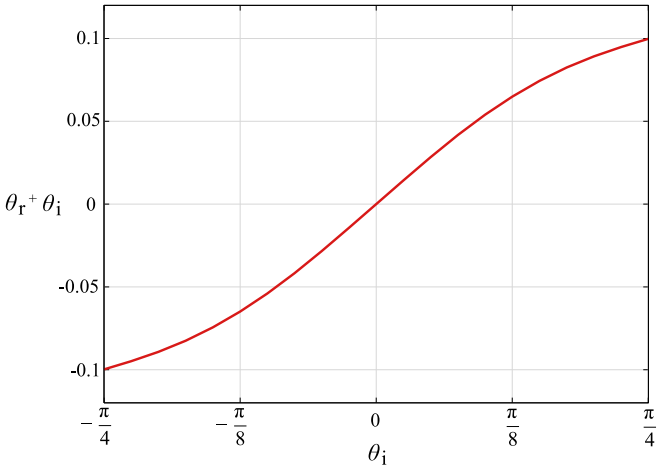


**FIGURE 8** The reflected angle plus the incident angle, $\theta_r + \theta_i$, as a function of the incident angle $\theta_i$. The deviation from the standard case, $\theta_r + \theta_i = 0$ for a non-Abelian system is clearly seen. The parameters were chosen to be $\kappa = 1$, $\Delta p = 1$ and initial momentum $|\boldsymbol{p}_0| = 8$

Figure 7 shows the reflection of the wavepacket for $\Delta p = \hbar\kappa$ (i.e., for momentum spreadings for which, as discussed above, the non-Abelian effects are significant). It is clear from the figures that the non-Abelian dynamics after the reflection is certainly not trivial. Remarkably, the center-of-mass position does not show in general a specular reflection. Figure 8 shows the sum of the angle of incidence and that of reflection for different incident angles in the non-Abelian regime. For usual scalar (or Abelian) evolution, this sum equals zero. However, due to inherently non-Abelian effects, this sum is significantly different from zero. Moreover, contrary to the usual scalar (or Abelian) evolution, the angle of reflection crucially depends on the absolute value of the incoming momentum, and on the momentum spreading of the wavepacket.

## 5 Conclusions

Summarizing, gauge fields may be generated using appropriate laser arrangements with atoms with degenerate internal states. Using a very simple laser configuration, spatially homogeneous but non-Abelian vector potentials can be generated. In spite of this spatial homogeneity, the non-Abelian character of the vector potentials can lead to a surprisingly rich physics for the wavepacket dynamics of ultracold gases. On one hand, the free expansion dynamics of wavepackets crucially differs from what would be expected in scalar (or Abelian) cases. In the latter, the wavepacket center-of-mass follows a linear dependence in time. In the presence of non-Abelian fields, the wavepacket presents a non-linear time dependence during a transient time. In addition, and again contrary to the scalar or Abelian case, the center-of-mass dynamics crucially depends on the momentum spreading of the wavepacket. Moreover, in spite of the apparent separability of the corresponding Hamiltonian, the non-Abelian gauge fields introduce a dependence of the dynamics in different spatial directions. The wavepacket reflection off an atomic mirror is also significantly distorted by the non-Abelian gauge field. In particular, the reflection of the center-of-mass ceases in general to be specular, and the angle of reflection depends on the incoming velocity and the initial momentum spreading, which is different from the standard scalar case. The complex interplay between external and internal dynamics should make the read-out of non-Abelian interferometers difficult. However, an experiment performed with optical tweezers may allow for the analysis of non-Abelian effects in the internal dynamics of the atoms. In particular, we have shown that such an arrangement can be employed for the analysis of the equivalent of the non-Abelian Aharanov–Bohm effect, where the final internal state of the atoms crucially depends on the particular path chosen.

**ACKNOWLEDGEMENTS** This work was supported by the Deutsche Forschungsgemeinschaft (SFB-TR21, SFB407, SPP1116), the European Graduate College "Interference and Quantum Applications", the UK Engineering and Physical Sciences Research Council, and the Royal Society of Edinburgh.

## REFERENCES

1 J.D. Jackson, *Classical Electrodynamics* (Wiley, New York, 2002)
2 C.A. Mead, Rev. Mod. Phys. **64**, 51 (1992)
3 O.D. Lavrentovich, JETP Lett. **43**, 382 (1986)
4 M.N. Chernodub, JETP Lett. **83**, 268 (2006)
5 F. Wilczek, A. Zee, Phys. Rev. Lett. **52**, 2111 (1984)
6 J. Ruseckas, G. Juzeliūnas, P. Öhberg, M. Fleischhauer, Phys. Rev. Lett. **95**, 010404 (2005)
7 K. Osterloh, M. Baig, L. Santos, P. Zoller, M. Lewenstein, Phys. Rev. Lett. **95**, 010403 (2005)
8 P.A. Horváthy, Phys. Rev. Lett. **95**, 010403 (2005)
9 R. Unanyan, M. Fleischhauer, B.W. Shore, K. Bergmann, Opt. Commun. **155**, 144 (1998)
10 R. Unanyan, B.W. Shore, K. Bergmann, Phys. Rev. A **59**, 2910 (1999)
11 D. McGloin, G.C. Spalding, H. Melville, W. Sibbett, K. Dholakia, Opt. Express **11**, 158 (2003)
12 G. Whyte, J. Courtial, New J. Phys. **7**, 117 (2005)
13 G. Juzeliūnas, P. Öhberg, Phys. Rev. Lett. **93**, 033602 (2004)
14 G. Juzeliūnas, J. Ruseckas, P. Öhberg, A. Klein, Phys. Rev. A **71**, 053614 (2005)
15 G. Juzeliūnas, J. Ruseckas, P. Öhberg, M. Fleischhauer, Phys. Rev. A **73**, 025602 (2006)
16 C.G. Aminoff, A.M. Steane, P. Bouyer, P. Desbiolles, J. Dalibard, C. Cohen-Tannoudji, Phys. Rev. Lett. **71**, 3083 (1993)
17 K. Bongs, S. Burger, G. Birkl, K. Sengstock, W. Ertmer, K. Rzążewski, A. Sanpera, M. Lewenstein, Phys. Rev. Lett. **83**, 3577 (1999)
18 A.S. Arnold, M.J. Pritchard, D.A. Smith, I.G. Hughes, New J. Phys. **8**, 53 (2006)